PHYSICAL REVIEW B VOLUME 61, NUMBER 9 1 MARCH 2000-I

Neutron-scattering study of the magnetic structure of $DyFe_4Al_8$ and $HoFe_4Al_8$

J. A. Paixão and M. Ramos Silva
Departamento de Física, University of Coimbra, P-3000 Coimbra, Portugal

S. Aa. Sørensen and B. Lebech
Condensed Matter Physics and Chemistry Department, P.O. Box 49, DK-4000 Roskilde, Denmark

G. H. Lander
European Commission, Joint Research Centre, Institute for Transuranium Elements, Postfach 2340, D-76125 Karlsruhe, Germany

P. J. Brown
Institut Laue-Langevin, Boîte Postale 156X, F-38042 Grenoble, France

S. Langridge
European Synchrotron Radiation Facility, Boîte Postale 220X, F-38043 Grenoble, France

E. Talik
Institute of Physics, University of Silesia, Katowice, Poland

A. P. Gonçalves
Instituto Tecnológico e Nuclear, P-2686 Sacavém, Portugal

(Received 22 September 1999)

The magnetic structures of $DyFe_4Al_8$ and $HoFe_4Al_8$, which have been reported to be unusual spin-glass systems, were studied in detail by neutron diffraction, using both unpolarized and polarized beams. In fact these compounds have long-range magnetic order in both the Fe and rare-earth sublattices. The Fe sublattice orders at 175 K with the moments $(1.0\mu_B)$ in the ab plane in a cycloid magnetic structure with a propagation vector along [110]. At ~ 50 K the rare-earth moment starts to order in $DyFe_4Al_8$ and follows the modulation of the Fe sublattice. The ordering of the holmium occurs at a slightly higher temperature (~ 80 K) than the dysprosium. At a lower temperature higher-order harmonics of the modulation develop. The magnetic structure of the rare-earth at low temperature is a bunched elliptical cycloid, following the modulation of the Fe sublattice. Although the antiferromagnetic coupling of the rare-earth magnetic moments has long-range order, giving sharp magnetic satellites in the diffraction patterns, a non-negligible fraction of the $4f$ moment does not contribute to these peaks but appears as diffuse scattering beneath the Bragg peaks. This indicates the presence of short-range ferromagnetic correlations between neighboring rare-earth moments. The magnetic structure of the rare-earth sublattice is very sensitive to a small applied magnetic field, mimicking spin-glass behavior in the bulk magnetic properties. The magnetic structure of $DyFe_4Al_8$ was studied under an applied magnetic field. A field as low as 0.125 T severely distorts the magnetic modulation and 0.75 T in the ab plane is sufficient to align all the rare-earth moments ferromagnetically. The cycloidal antiferromagnetic coupling of the Fe moments remains unperturbed up to at least 5 T.

I. INTRODUCTION

The magnetic properties of ternary intermetallic compounds with the $ThMn_{12}$ type of structure and composition $M\,Fe_{12-x}X_x$ where M is a rare earth or actinide atom and X a p-element (Al, Si) continue to attract much interest, mainly because the compounds with higher Fe content like $SmFe_{10}Si_2$ are ferromagnets with high Curie temperatures ($T_C \sim 600$ K) and a relatively large magnetic anisotropy. The rare-earth sublattice provides the required anisotropy and the high T_C is due to the strong Fe-Fe exchange interaction. The stoichiometric compounds of composition $M\,Fe_4Al_8$ exhibit interesting magnetic properties whose interpretation has remained controversial.

The crystal structure is tetragonal body centered with the space-group $I4/mmm$. The unit cell is shown in Fig. 1. The M atoms are located at the $2a$ sites at the origin and center of the unit cell. For the stoichiometric $M\,Fe_4Al_8$ compounds the Fe atoms ideally occupy only the $8f$ positions and in this case the M atoms are at the centers of tetragonal prisms which have the Fe atoms as vertices. With increasing Fe content the transition metal atoms occupy also the $8i$ and $8j$ positions, mixing with the Al atoms. The high Fe-content compounds are ferromagnetic, but the ground states of the $M\,Fe_4Al_8$ compounds cannot be easily determined from their bulk properties. Although a number of techniques have been used to study these materials, a very confusing and sometimes contradictory picture of the magnetic properties emerges from the published literature.

In the first study of the magnetic properties of $M\,Fe_4Al_8$

0163-1829/2000/61(9)/6176(13)/$15.00

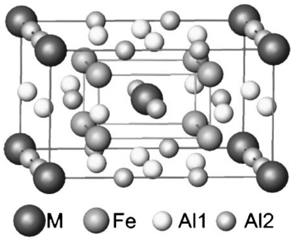

FIG. 1. Unit cell of $M\mathrm{Fe}_4\mathrm{Al}_8$. The rare-earth atoms ($M$) are the origin and center of the unit cell in a cage formed by the 8 Fe atoms at the $8f$ sites.

compounds, Buschow and van der Kraan[1] report bulk magnetization and Mössbauer measurements for a number of compounds in this family. In the curves of susceptibility vs temperature a maximum is observed for all compounds in the temperature range $100<T<200$ K, which was interpreted as the onset of antiferromagnetic ordering of the Fe sublattice. In the cases of $M=\mathrm{Y}$, La, Ce, Lu, and Th compounds, there is no ordered moment on the M atom and no further anomalies in the susceptibility are observed at low temperature. For the other compounds it was deduced, on the basis of susceptibility and magnetization data, that the rare earth moments order at low temperature ($T<35$ K). For many compounds the low-temperature susceptibility is strongly dependent on the field and annealing treatment during sample preparation. These effects were attributed to partial disorder between the Fe and Al atoms. From the Mössbauer measurements, the ordering temperatures of the Fe sublattice are found in the range $135<T_N<200$ K for all compounds of this series. The long-range ordering of the rare-earth moment occurs at a much lower temperature, below 50 K. The reason why the rare-earth orders at such low temperatures, despite an M-Fe interaction estimated as roughly half that between Fe moments,[1] was thought to be due to the fact that any simple antiferromagnetic arrangement of the Fe moments gives zero molecular field at the M site. Because of the symmetrical arrangement of the 8 Fe atoms surrounding the M atom their individual contributions cancel out. Direct M-M interaction is negligible, as shown by the isostructural compounds containing Mn atoms carrying no moment, which are paramagnetic down to very low temperatures.

These results were confirmed by Felner and Nowik[2] who suggested that the ordering of the M moments is antiferromagnetic on the basis of the relatively small moments that can be induced by field at low temperature. Furthermore, these authors point out that the ^{57}Fe Mössbauer spectra of $\mathrm{GdFe}_4\mathrm{Al}_8$ suggests that the Fe sublattice may not order as a simple antiferromagnet.

The magnetism of $\mathrm{DyFe}_4\mathrm{Al}_8$ has also been studied by ^{161}Dy Mössbauer spectroscopy.[3] The data are poor, due to the fact that the Dy resonance is broad and the sources are weak. Using a rather involved method of data analysis, the authors conclude that in $\mathrm{DyFe}_4\mathrm{Al}_8$ the Dy sublattice orders at (43 ± 8) K with the moments aligned along the crystallographic c axis.

So far, the only reported neutron study of $\mathrm{DyFe}_4\mathrm{Al}_8$ was performed on a polycrystalline sample.[4] In this study, the isostructural compound $\mathrm{HoFe}_4\mathrm{Al}_8$ was also investigated. In both cases, magnetic peaks in the form of weak satellites were found at temperatures below 25 K around a few nuclear Bragg reflections, with a propagation vector parallel to the (110) reciprocal lattice vector. Based on their failure to observe magnetic peaks at higher temperature, these authors proposed a model in which the Fe moments only order below 25 K, despite the fact that Mössbauer and susceptibility measurements show that Fe is ordered at ~180 K. They proposed a conical spiral structure in which the Dy moments do not have long-range magnetic order but freeze in a ‘‘spin-glass’’ state.

A few years later, Gal *et al.*[5,6] reported a study of $\mathrm{HoFe}_4\mathrm{Al}_8$ in which a number of techniques were employed, including ac and dc susceptibility measurements, ^{57}Fe Mössbauer spectroscopy and powder neutron diffraction. It was claimed that $\mathrm{HoFe}_4\mathrm{Al}_8$ exhibits some of the irreversible and time-dependent characteristics of a spin glass. Although the observation of satellites in the neutron diffraction pattern at temperatures below 180 K is briefly mentioned in the text, it is claimed that the Fe moments order only at 20 K. The hyperfine field on the Fe nuclei appears at 175(5) K but this was interpreted as an indication of local ordering only. In the powder neutron-diffraction study, they observed a nonreproducible ferromagnetic ordering of the Ho moments at low temperature when applying a field, and hysteretic behavior when the field was removed.

The idea of a spin-glass system was further developed by Talik *et al.*[7,8] who report resistivity, ac and dc susceptibility and magnetization measurements on single crystals of $\mathrm{DyFe}_4\mathrm{Al}_8$ and $\mathrm{HoFe}_4\mathrm{Al}_8$. An antiferromagnetic transition was visible for both compounds at 180 K and below 40 K the susceptibility was strongly dependent on the way the crystal was cooled. A sharp maximum in the dc susceptibility was found at 30 K and a smaller anomaly at ~10 K was visible for fields applied parallel to the c axis. Both compounds have strongly anisotropic magnetic properties and measurements performed along the c and a axes showed that a is the easy axis. Measurements in high fields on $\mathrm{HoFe}_4\mathrm{Al}_8$ gave a saturation moment of $8.5\mu_\mathrm{B}/\mathrm{f.u.}$ and a remanence of $6.5\mu_\mathrm{B}/\mathrm{f.u.}$. The antiferromagnetic interaction in the Fe sublattice seems to be stable up to at least 14 T. The existence of a cusp in the ac susceptibility at 10 and 30 K for the Ho and Dy compounds, respectively, and the thermomagnetic history effects were again considered as an indication of spin-glass behavior.

$\mathrm{UFe}_4\mathrm{Al}_8$ (Ref. 9) is another system which was claimed to be a spin glass. It also showed peculiar bulk properties, including hysteresis in the thermomagnetic curves and an ac susceptibility cusp. We have recently reported[10] a single-crystal neutron-diffraction study of $\mathrm{UFe}_4\mathrm{Al}_8$ that proved that this compound is actually a canted ferrimagnet which has long-range magnetic order in both the U and Fe sublattices.

It is clear from these contradictory results and the unusual models proposed to interpret them that microscopic techniques employing single-crystal samples are needed when dealing with these systems. We have therefore engaged on a research project to investigate the magnetic structures of ThMn_{12}-type compounds using single-crystal neutron and magnetic x-ray diffraction.

II. SAMPLE CHARACTERIZATION

All experiments reported in this paper were performed on two single crystals grown by the Czochralski method from

TABLE I. Structural parameters of $DyFe_4Al_8$ and $HoFe_4Al_8$ determined from the least-squares refinement of 4-circle nuclear intensity data ($\lambda=1.047$ Å). The site labels refer to the Wyckoff notation, B is the Debye-Waller factor, and O_c is the site occupation factor. Cell parameters (room temperature): $DyFe_4Al_8$, $a=b=8.731$ Å, $c=5.039$ Å; $HoFe_4Al_8$, $a=b=8.669$ Å, $c=5.005$ Å.

Atom	Site	x	y	z	B(Å^2)	Oc
Dy	$2a$	0	0	0	0.37(4)	1.00[a]
Fe	$8f$	$\frac{1}{4}$	$\frac{1}{4}$	$\frac{1}{4}$	0.42(5)	0.99(1)
Al_I	$8i$	0.3414(5)	0	0	0.54(6)	0.95(2)
Al_{II}	$8j$	0.2794(5)	$\frac{1}{2}$	0	0.47(7)	0.96(3)
Ho	$2a$	0	0	0	0.58(6)	1.00[b]
Fe	$8f$	$\frac{1}{4}$	$\frac{1}{4}$	$\frac{1}{4}$	0.45(5)	0.99(2)
Al_I	$8i$	0.3418(3)	0	0	0.48(8)	0.96(2)
Al_{II}	$8j$	0.2787(3)	$\frac{1}{2}$	0	0.33(8)	0.98(2)

[a] Fixed during refinement.

[b] Fixed during refinement.

the levitated melt using high purity starting materials. The $DyFe_4Al_8$ crystal is the same sample that was used for the previously reported resonant x-ray magnetic scattering (RXMS) experiment.[11]

Although the crystallographic structure was known previously, a careful characterization of the samples by neutron diffraction was undertaken to check for extinction effects and also to rule out possible disorder between the Al and Fe positions. The experiment was performed on the 4-circle neutron diffractometer TAS2 at Risø which is installed on a thermal neutron beam ($\lambda=1.047$ Å). A total of ~500 reflections was measured at room temperature for each compound, up to $\sin\theta/\lambda=0.6$ Å^{-1}. These intensities were used for a least-squares refinement of the crystallographic structure. Both absorption (in the case of the Dy compound) and extinction were included in the refinement. The extinction model was that of Becker-Coppens[12] (isotropic, type I) with a Lorentzian mosaic distribution. The residual difference between the calculated and observed scattering amplitudes was $R(F)=2.7\%$ for the crystal of $DyFe_4Al_8$ and 3.3% for that of $HoFe_4Al_8$. The results of the structure refinements are shown in Table I. They confirm the good quality of both crystals and also confirm that the Fe and Al sublattices are well ordered in our samples. Extinction is not negligible at this wavelength for either compound but could be satisfactorily corrected by the extinction model. The crystal of $DyFe_4Al_8$ had a slightly smaller mosaic spread (0.65′) than that of $HoFe_4Al_8$ and for the former crystal there was a reduction of 30% in the intensity of the strongest Bragg reflection due to extinction, although on average the intensity loss was only 5%.

The magnetic susceptibility and magnetization curves of two small single crystals ($m\sim5\times10^{-3}$ g) cut from the big samples used for the neutron experiments were measured on a QUANTUM-DESIGN MPMS magnetometer. The measurements were performed in fields up to 5.5 T applied parallel to the a and c axes.

In agreement with previous measurements[7] we have found that $DyFe_4Al_8$ and $HoFe_4Al_8$ have an easy ab plane of magnetization, and observed a pronounced difference between the ZFC and FC susceptibility curves. The ZFC low-field susceptibility shows a maximum at 25 K and a further small anomaly at 10 K.

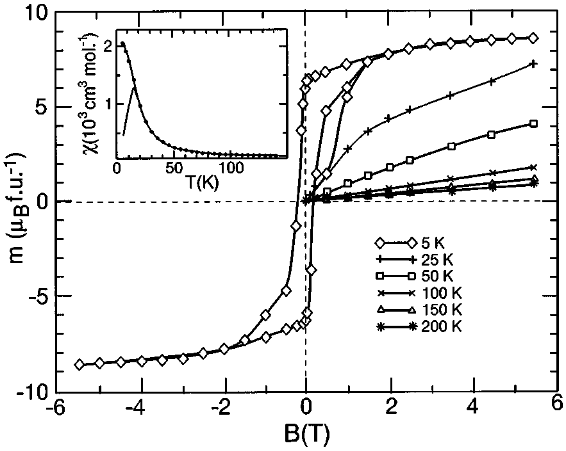

FIG. 2. Magnetization curves measured on a single crystal $DyFe_4Al_8$ with an applied field parallel to the a axis at 5 temperatures: 5 K (◇),25 K(+),50 K(□), 100 K(×), 150 K(△), and 200 K(*) For the lowest temperature the full hysteresis cycle is shown. The inset shows the susceptibility measured in a field of 250 Oe$\|a$ as a function of temperature; ●: field cooled measurements; solid line: zero field cooled.

A set of magnetization curves of $DyFe_4Al_8$ at different temperatures and the full hysteresis cycle at 4.2 K for $H\|a$ are shown in Fig. 2. Above 50 K the magnetization increases linearly with the field, which is typical of antiferromagnetism, but at 25 K the magnetization curve deviates significantly from linearity. At 4.2 K a remanence of $6.7\mu_B$/f.u. is measured and the magnetization is almost saturated in a field of 5.5 T. The total aligned magnetic moment is $8.6\mu_B$, which is close to the full moment of the rare-earth. When the field is applied along the c-axis the magnetization is small and linear with the field, and no hysteresis is observed.

III. MAGNETIC STRUCTURE

A. Unpolarized neutrons

The first crystal examined with neutrons was $DyFe_4Al_8$. A survey experiment to investigate the magnetic structure was performed on the 4-circle TAS2 diffractometer at Risø, following the data collection at room temperature to refine the crystallographic structure. The crystal was inserted in a closed-cycle helium refrigerator reaching a minimum temperature of 20 K. A search for magnetic reflections was performed by scanning along the main reciprocal lattice lines. At temperatures below 175 K satellites were found around the h and k odd reflections along the 110 and $1\bar{1}0$ directions. The propagation vector is $\tau\tau0$ with $\tau=0.133\sim2/15$ r.l.u. There are two pairs of satellites around each nuclear reflection, each pair corresponding to one of the two configuration domains generated by the crystallographic fourfold axis that does not belong to the magnetic group.

These satellites arise from long-range ordering of the Fe moments in a modulated structure, and provide direct evidence against the spin-glass state for the Fe moments which it has been suggested exists between 20 K and 180 K.[4] These satellite peaks are narrow, with a width comparable with that of the nuclear reflections and they are relatively weak in this temperature region; this is certainly why they have not been previously reported in powder neutron-diffraction experiments.[4]

The selection rule h and k odd arises because the Fe atoms occupy the special positions $8f$. When these atoms are scattering in phase they only contribute to h even, k even, l even reflections. The magnetic ordering lowers the crystallographic site symmetry and removes the fourfold axis which splits the Fe lattice into two nonequivalent sublattices. The fact that the Fe satellites are only observed around h and k odd reflections means that the magnetic modulations of these two nonequivalent Fe sublattices are 180° out of phase.

The intensities of the $110^{\pm}$ satellites were followed as function of temperature while cooling the crystal. At around 50 K, the $I(T)$ curve showed a pronounced upturn and at the base temperature of the closed-cycle cryostat (20 K) weak satellites corresponding to the same propagation vector could also be observed around reflections with h and k even or h and k indices of different parity and l odd, which are forbidden for the Fe sublattice. These are attributed to the onset of magnetic ordering of the Dy atoms which are located at the origin and center of the unit cell and thus contribute to every point ($h+k+l$ even) of the reciprocal lattice. Satellites were never observed around reflections which violate the body centering rule.

Following this survey, more detailed experiments were performed on both $DyFe_4Al_8$ and $HoFe_4Al_8$ with the D10 4-circle diffractometer at the Institut Laue-Langevin (ILL). This diffractometer is installed on a thermal neutron guide and combines a particularly low background and high flux with good momentum resolution, both of which are needed for accurate measurement of the magnetic satellites. Most of the data were collected using a PG (002) monochromator ($\lambda = 2.36$ Å) with a $\lambda/2$ filter in the incoming beam, although some data on $DyFe_4Al_8$ were also measured with a shorter wavelength ($\lambda = 1.32$ Å) using a Cu (220) monochromator. The sample was mounted inside the D10 helium-flow cryostat which can cool the sample down to a temperature of 1.5 K while maintaining full 4-circle capability of the instrument.

A reciprocal lattice scan along the $hh0$ direction through 121 is shown in Fig. 3 for various temperatures. This reflection is sensitive only to the ordering of the Dy sublattice. Below 10 K, high-order harmonics of the modulation develop and are clearly visible up to the 7th order in the low-temperature scans. A broad pattern of diffuse scattering, which appears at the same temperature as the high-order harmonics, can also be seen beneath the nuclear peaks. It extends right across the Brillouin zone (see Sec. VIII).

The scans around the h and k odd reflections, which are sensitive to the ordering of *both* the Dy and Fe sublattices, show the same higher-order satellites and diffuse scattering pattern at low temperature. The higher-order satellites and diffuse scattering disappear simultaneously at 10 K, but the 1st order satellite remains visible up to 175 K.

In Fig. 4 is shown the temperature dependence of the modulation vector of $DyFe_4Al_8$ obtained from longitudinal scans through the 110 reflection. The period of the modulation appears to change with temperature in a continuous way and at about 20 K it levels out to a value close to 0.133(1), suggesting that the low-temperature value of the modulation is a rational number $\frac{2}{15}$. It corresponds to a rotation by 48° when going from one Dy layer to the next along a [110] direction.

The evolution with temperature of the intensity of the satellites around a Dy only reflection 121 and a mixed Fe/Dy reflection 110 are shown in Fig. 5. The intensity of the first-order satellite starts to increase at around 50 K and rises sharply below 25 K. At 10 K, with the onset of the higher-order satellites, a decrease in the intensity of the first order was observed.

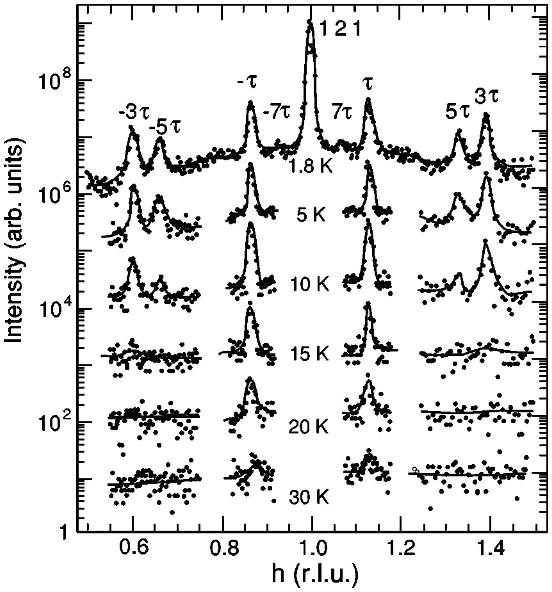

FIG. 3. Reciprocal lattice scans of $DyFe_4Al_8$ along the (110) direction passing through the 121 Bragg reflections for various temperatures. This Bragg point is forbidden for the Fe modulation and the magnetic satellites seen at low temperature originate from the rare-earth moment only. The base lines of successively higher temperature scans are offset by factors of 10^2. Data measured on D10 at ILL $\lambda = 2.36$ Å.

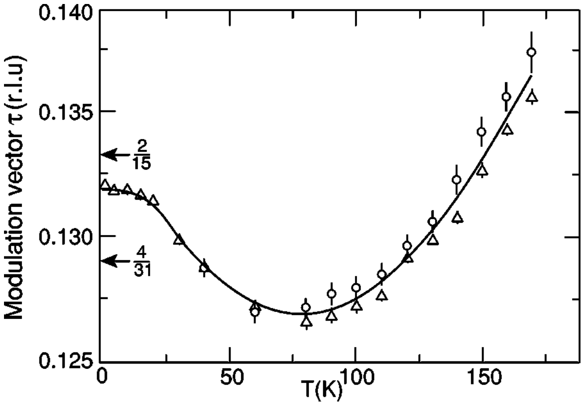

FIG. 4. Evolution with temperature of the wave vector modulating the magnetic structure of $DyFe_4Al_8$ as measured on the D10 diffractometer. Open circles (open triangles) are determined by longitudinal (transverse) scans. The commensurate positions of $\frac{4}{31}$ and $\frac{2}{15}$ are marked. (See Ref. 16 for further details.)

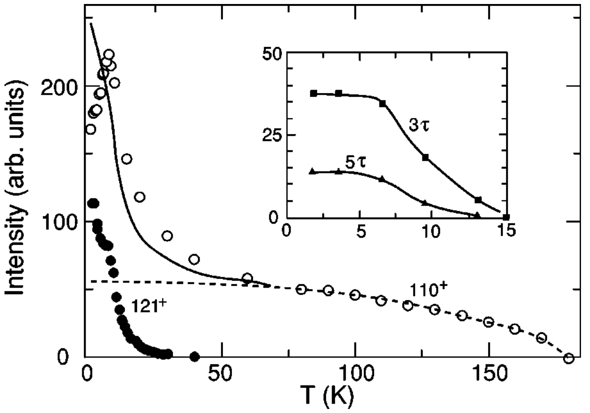

FIG. 5. Temperature dependence of the intensity of the first order satellites around the reflections 121 and 110 of $DyFe_4Al_8$. The temperature dependence of the third and fifth order satellites of the 121 reflection is shown on the inset. The solid line is the calculated temperature dependence of the 110^+ satellite using the model discussed in the text. The dashed line is the contribution to the 110^+ originating from the Fe sublattice only.

The magnetic order in $HoFe_4Al_8$ has many similarities with that of $DyFe_4Al_8$. The $\boldsymbol{\tau}$ vector is along (110) as in $DyFe_4Al_8$, but its modulus is slightly larger [$\tau = 0.142(2)$ r.l.u.]. The higher-order satellites of the modulation are not as intense as in $DyFe_4Al_8$, the fifth-order satellite was barely visible although the third was clearly seen. Also, less diffuse scattering is present at low temperature. Despite these similarities, there is a striking difference in the evolution with temperature of the intensity of the first order harmonic of a mixed Fe+Ho satellite as is shown in Fig. 6. When the rare-earth sublattice starts to order as shown by the appearance of the 121 satellites at ~55 K, the intensities of the 110 satellites *decrease* with temperature, down to a minimum at 23 K subsequently increasing as the temperature is lowered further to 1.5 K. This behavior is the reverse of that observed in $DyFe_4Al_8$ and is reproducible in both heating and cooling cycles with no hysteresis.

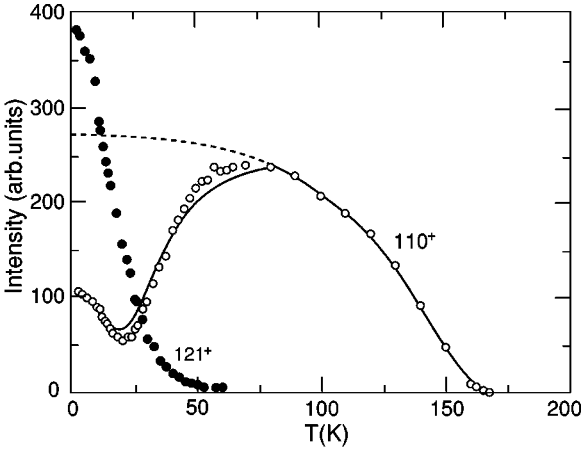

FIG. 6. Temperature dependence of the intensity of the first order satellites around the reflections 121 and 110 of $HoFe_4Al_8$. The solid line is the calculated temperature dependence of the 110^+ satellite using the model discussed in the text. The dashed line is the contribution to the 110^+ originating from the Fe sublattice only.

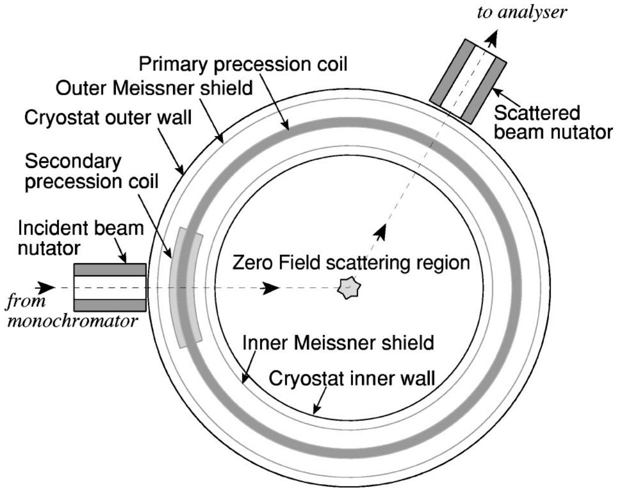

FIG. 7. Horizontal section through the CRYOPAD polarimeter. The polarization of the incident neutrons is guided by the *incident beam nutator* so as to emerge an angle θ to the vertical (z) in a plane perpendicular to their wave vector. Between *the inner and outer Meissner shields* the neutron polarization precesses by an angle χ around the horizontal field due to both the *primary and secondary precession coils.* The currents in the coils are adjusted so that when the neutrons enter the central *zero-field scattering region* their polarization is in the chosen direction. The precession and nutation angles which guide the polarization of the scattered beam into the direction accepted by the analyzer, are controlled in a similar way.

B. Spherical polarimetry

Zero-field neutron polarimetry was carried out using the 3D neutron-polarimeter CRYOPAD II[13] installed on the sample table of the polarized-neutron triple-axis spectrometer IN20 at the ILL. The crystal was mounted with the $[1\bar{1}0]$ direction vertical inside an ILL orange cryostat placed in the annular zero-field space of CRYOPAD II (Fig. 7) For a selection of hhl reflections the direction of the scattered polarization was determined with the incident polarization successively parallel to the vertical direction (z), the scattering vector $\boldsymbol{\kappa}(x)$ and a third direction (y) that completes the right-handed Cartesian set. The xyz axes are the polarization axis and from their definition the magnetic interaction vector $\mathbf{Q}$ lies in the yz plane, since it is perpendicular to $\boldsymbol{\kappa}$. (The use of $\mathbf{Q}$ for the magnetic interaction vector follows Ref. 13 but care should be taken not to confuse this with the scattering vector $\boldsymbol{\kappa}$. The magnetic interaction vector is the projection of the Fourier transform of the magnetization $\mathbf{M}(\mathbf{r})$ onto the plane perpendicular to $\boldsymbol{\kappa}$. $\mathbf{Q} = \hat{\boldsymbol{\kappa}} \times \int \mathbf{M}(\mathbf{r}) e^{i\boldsymbol{\kappa}\cdot\mathbf{r}} d^3r \times \hat{\boldsymbol{\kappa}} = \mathbf{M}(\boldsymbol{\kappa}) - [M(\boldsymbol{\kappa}) \cdot \hat{\boldsymbol{\kappa}}]\hat{\boldsymbol{\kappa}}$, where $\hat{\boldsymbol{\kappa}}$ is a unit vector in the direction of the scattering vector and $\mathbf{M}(\boldsymbol{\kappa})$ is the Fourier transform of the magnetization.)

The measurements were performed with a neutron wavelength of 2.36 Å at the temperatures of 1.5 K, 17 K, and 50 K. For the lowest temperature polarimetric data on the first and third order satellites of reflections 002, 222, 110 and 112 and the fifth order satellite of 002 were measured. At 17 K only the first order satellite was measured, and at 50 K the measurement was performed on the 110 and 112 reflections only, which are those sensitive to the Fe ordering. The

TABLE II. CRYOPAD polarimetric data for the first order satellites of $DyFe_4Al_8$. P_i and P_f are the polarization vectors of the incident and diffracted beams. The polarization axis are $x\|\boldsymbol{\kappa}$, z is vertical and parallel to $[1\bar{1}0]$ and y is in the scattering plane, defining with x and z a right handed orthogonal set. P_c is the calculated polarization from the magnetic structure model discussed in the text. The estimated error bars for the incident and scattered polarizations are 0.01 and 0.03, respectively.

	P_i			P_f			P_c	
x	y	z	x	y	z	x	y	z
				50 K				
110^+								
0.90	0.00	0.00	−0.86	−0.04	0.04	−0.90	0.00	0.00
0.00	0.90	0.00	0.10	−0.88	0.00	0.00	−0.90	0.00
0.00	0.00	0.90	0.01	−0.04	0.88	0.00	0.00	0.90
112^+								
0.90	0.00	0.00	−0.87	−0.11	−0.07	−0.92	0.00	0.00
0.00	0.90	0.00	0.13	−0.18	0.12	−0.01	−0.19	0.00
0.00	0.00	0.90	0.02	0.03	0.17	−0.01	0.00	0.19
				17 K				
110^+								
0.00	0.90	0.00	0.06	−0.89	0.02	0.00	−0.90	0.00
0.00	0.00	−0.90	−0.05	−0.02	−0.89	0.00	0.00	−0.90
112^+								
0.90	0.00	0.00	−0.93	−0.07	−0.04	−1.00	0.00	0.00
0.00	0.90	0.00	−0.03	0.38	0.05	−0.05	0.35	−0.02
0.00	0.00	0.90	−0.15	−0.05	−0.30	−0.05	−0.02	−0.35
112^-								
0.90	0.00	0.00	−0.89	0.07	0.01	−0.81	0.00	0.00
0.00	0.90	0.00	0.23	0.35	0.05	0.05	0.38	−0.02
0.00	0.00	0.90	0.14	0.10	−0.32	0.05	−0.02	−0.38
				1.8K				
110^+								
0.90	0.00	0.00	−0.91	−0.09	0.04	−0.90	0.00	0.00
0.00	0.90	0.00	0.07	−0.90	0.02	0.00	−0.90	0.00
0.00	0.00	0.90	−0.01	−0.01	0.93	0.00	0.00	0.90
112^+								
0.90	0.00	0.00	−0.85	0.29	−0.04	−0.90	0.00	0.00
0.00	0.90	0.00	0.03	0.49	0.03	−0.00	0.49	0.01
0.00	0.00	0.90	0.06	−0.07	−0.48	−0.00	0.01	−0.49
112^-								
0.90	0.00	0.00	−0.91	0.10	−0.01	−0.90	0.00	0.00
0.00	0.90	0.00	−0.04	0.54	0.03	0.00	0.52	0.01
0.00	0.00	0.90	−0.02	0.08	−0.53	0.00	0.01	−0.52
002^+								
0.90	0.00	0.00	−0.91	0.08	−0.01	−0.93	0.00	0.00
0.00	0.90	0.00	0.12	−0.36	−0.01	−0.02	−0.39	0.00
0.00	0.00	0.90	−0.01	0.03	0.42	−0.02	0.00	0.39
222^+								
0.00	0.90	0.00	0.08	−0.55	−0.02	−0.01	−0.57	0.00
0.00	0.00	0.90	0.05	−0.19	0.52	−0.01	0.00	0.57

(fixed) incident and (measured) scattered polarizations of this set of reflections are shown in Table II.

IV. ANALYSIS OF THE DATA

For a pure magnetic reflection, the cross section for Bragg scattering of a beam of neutrons with polarization $\mathbf{P}_i$ is[14]

$$\frac{\partial\sigma}{\partial\Omega}=\mathbf{Q}\cdot\mathbf{Q}^*+i\mathbf{P}_i(\mathbf{Q}^*\times\mathbf{Q}) \tag{4.1}$$

and the scattered polarization $\mathbf{P}_s$ is

$$\mathbf{P}_s\frac{\partial\sigma}{\partial\Omega}=\mathbf{Q}(\mathbf{P_i}\cdot\mathbf{Q}^*)+\mathbf{Q}^*(\mathbf{P_i}\cdot\mathbf{Q}^*)-\mathbf{P}_i^*(\mathbf{Q}\cdot\mathbf{Q}^*)-i(\mathbf{Q}^*\times\mathbf{Q}). \tag{4.2}$$

For an amplitude modulated wave the magnetic moment on the jth atom of the lth unit cell may be written

$$\mathbf{S}_{jl}=\mathbf{A}_j\cos(\boldsymbol{\tau}\cdot\mathbf{r}_l+\phi_j) \tag{4.3}$$

and for a helix or cycloidal magnetic structure

$$\mathbf{S}_{jl}=\mathbf{A}_j\cos(\boldsymbol{\tau}\cdot\mathbf{r}_l+\phi_j)+i\mathbf{B}_j\sin(\boldsymbol{\tau}\cdot\mathbf{r}_l+\phi_j), \tag{4.4}$$

where for this case $\mathbf{A}_j$ and $\mathbf{B}_j$ are perpendicular vectors giving the magnitude and direction of the major and minor axis of the elliptical envelope of the spin modulation on the jth atom, $\boldsymbol{\tau}$ is the propagation vector of the modulation, and $\mathbf{r}_l$ the vector defining the origin of the lth unit cell. The phases of the modulations of the magnetic atoms are given by ϕ_j. The corresponding magnetic interaction vector is

$$\mathbf{Q}(\boldsymbol{\kappa})=\hat{\boldsymbol{\kappa}}\times\left\{p\sum_{lj}\mathbf{S}_{jl}f_j(\boldsymbol{\kappa})\exp[i\mathbf{k}\cdot(\mathbf{r}_j+\mathbf{r}_l)]\right\}\times\hat{\boldsymbol{\kappa}}. \tag{4.5}$$

The $f_j(\boldsymbol{\kappa})$ functions are the magnetic form factors of the magnetic atoms, $\hat{\boldsymbol{\kappa}}$ is a unit vector in the direction of the scattering vector $\boldsymbol{\kappa}$ and the sum is over all magnetic atoms and all unit cells. $p=1/2\gamma r_0=0.2695\times10^{-12}$ cm is the magnetic scattering amplitude associated with $1\mu_{\mathrm{B}}$.

The sum over the cells can be carried out in the usual way giving

$$\mathbf{Q}(\boldsymbol{\kappa})=(\mathbf{C}\pm i\mathbf{D})\,\delta(\mathbf{G},\boldsymbol{\kappa}\pm\boldsymbol{\tau}), \tag{4.6}$$

where $\mathbf{G}$ is a reciprocal lattice vector and

$$\mathbf{C}=\hat{\boldsymbol{\kappa}}\times\sum_i\,pf_j(\boldsymbol{\kappa})\frac{\mathbf{A}_j}{2}\exp[i\boldsymbol{\kappa}\cdot(\mathbf{r}_j+\phi_j)]\times\hat{\boldsymbol{\kappa}}, \tag{4.7}$$

$$\mathbf{D}=\hat{\boldsymbol{\kappa}}\times\sum_i\,pf_j(\boldsymbol{\kappa})\frac{\mathbf{B}_j}{2}\exp[i\boldsymbol{\kappa}\cdot(\mathbf{r}_j+\phi_j)]\times\hat{\boldsymbol{\kappa}}. \tag{4.8}$$

For the simple case where only one magnetic sublattice exists, the cross section for the amplitude modulated wave may be written in the form

$$\frac{\partial\sigma}{\partial\Omega}=p^2A^2f(\boldsymbol{\kappa})^2\,\frac{1-\cos^2\Psi}{4}\,|F(\boldsymbol{\tau})|^2\,\delta(\mathbf{G},\boldsymbol{\kappa}\pm\boldsymbol{\tau}) \tag{4.9}$$

and for a cycloid where $|\mathbf{A}|=|\mathbf{B}|$

$$\frac{\partial\sigma}{\partial\Omega}=p^2f(\boldsymbol{\kappa})^2A^2\,\frac{1+\cos^2\Psi}{4}\,|F(\boldsymbol{\tau})|^2\,\delta(\mathbf{G},\boldsymbol{\kappa}\pm\boldsymbol{\tau}), \tag{4.10}$$

where $F(\boldsymbol{\tau})=\Sigma_j\exp(i\boldsymbol{\kappa}\cdot\mathbf{r}_j)$ is the geometrical structure factor of the jth sublattice. Here, Ψ is the angle between the momentum transfer vector $\boldsymbol{\kappa}$ and either the direction along which the magnetic moments are oriented in the case of an amplitude modulated wave or the normal to the plane in which the moments are rotating, in the case of a cycloid. Because of the different geometrical factors involving the angle Ψ, it is in principle possible to distinguish between these two types of magnetic structures by an accurate measurement of a set of magnetic reflections with various momentum transfers.

A more stringent test to differentiate between a modulation of the amplitudes and a modulation of the direction of the moments (helix) can be made if the change in polarization state of the neutrons scattered by the magnetic reflections can be determined. Analysis of Eq. (4.2) shows that the polarization ($\mathbf{P}_s$) of neutrons scattered by a pure magnetic reflection with $\mathbf{Q}\|\mathbf{Q}^*$ is related to the incident polarization, $\mathbf{P}_i$, by precession through 180° about the magnetic interaction vector $\mathbf{Q}$. The situation is different when $\mathbf{Q}$ and $\mathbf{Q}^*$ are not parallel, which happens in helical structures. In this case, if $\mathbf{P}_i$ is perpendicular to $\boldsymbol{\kappa}$ then the polarization is flipped around the longer component of $\mathbf{Q}$ and rotated towards the scattering vector by an angle which depends on the quantity $2\boldsymbol{\kappa}\cdot(\mathbf{A}\times\mathbf{B})/(A^2+B^2)$.[13]

In practice, one has to consider the existence of magnetic domains in the calculation of both the cross section and the scattered polarization.[15] In a multidomain sample, both the cross section and the scattered polarization have to be calculated for every magnetic domain and summed up with weights proportional to the domain fractions. In the case of a helix there are also chirality domains. It should be noted that a cycloidal structure does not have an *absolute* chirality since the sense of a cycloid is reversed by rotation of $\pi/2$ about its propagation direction. The apparent chirality of the structure is therefore reversed by this rotation and will appear to be opposite for the $h+\tau,k+\tau,l$ and $k+\tau,h+\tau,-l$ reflections. If the two *chirality* domains are equally populated the polarization along $\pm\boldsymbol{\kappa}$ is preserved in magnitude and reversed and polarization in the plane perpendicular to $\mathbf{Q}$ precesses around the longer component of $\mathbf{Q}$, its magnitude depending on $|\mathbf{A}^2-\mathbf{B}^2|$. Thus, if $|\mathbf{A}|=|\mathbf{B}|$, incident polarization in the plane perpendicular to $\boldsymbol{\kappa}$ is totally destroyed. By measuring the degree of depolarization of different Bragg reflections one may determine the ellipticity of the envelope of the modulation, i.e., the ratio between its major and minor axes.

It is simplest to start by analyzing the CRYOPAD data measured at 50 K to which only Fe moments contribute. The polarization scattered by the 110^+ reflection is not rotated when it is parallel to z ($[1\bar{1}0]$) but is reversed when parallel to either x $[(110)]$ or y ($[001]$). There is no significant depolarization of the beam in any of the three cases. This behavior is unique to the situation where the magnetic interaction vector $\mathbf{Q}$ is parallel to the z axis. For DyFe$_4$Al$_8$ this means that the Fe moments must lie in the ab crystallographic plane. Any component of the Fe moments along c is therefore excluded by data from a single reflection, which shows the power of the polarimetric technique. The polarimetric data for the 112^+ reflection show that there is severe depolarization of the beam except when the incident polarization is parallel to the scattering vector (x), in which case the outgoing polarization is simply reversed. This behavior is consistent with a cycloidal structure with moments rotating in the ab plane. A model corresponding to an amplitude modulated wave with moments pointing in a unique direction in the ab plane would not explain the observed depolarization in the y and z directions. The measured polarizations can be fitted to a cycloidal structure using Eq. (4.2). It was argued earlier that the selection rule for the Fe satellites, which are only observed around reflections with h and k odd, implies that the two nonequivalent Fe sublattices are 180° out of phase. The phases, relative to the origin of the unit cell, of the four Fe sublattices are

$$\mathrm{Fe1}\left(\frac{1}{4}\,\frac{1}{4}\,\frac{1}{4}\right)\psi=\tau\pi,\qquad \mathrm{Fe2}\left(\frac{3}{4}\,\frac{3}{4}\,\frac{1}{4}\right)\psi=3\tau\pi,$$

$$\mathrm{Fe3}\left(\frac{1}{4}\,\frac{3}{4}\,\frac{1}{4}\right)\psi=2\tau\pi+\pi,\qquad \mathrm{Fe4}\left(\frac{3}{4}\,\frac{1}{4}\,\frac{1}{4}\right)\psi=2\tau\pi+\pi. \tag{4.11}$$

It should be noted that the symmetry of the Fe and Dy sites does not restrict the envelope of the modulation to be circular; it may well have axes of different length. However, the symmetry of the problem *does* imply that if it is elliptical either the major or minor axis is parallel, and the other perpendicular, to the propagation vector. Table II gives the calculated values of the polarization of the scattered beam for this model together with the measured values. For the data at 50 K, the fit to the data has only two parameters, the relative population of the two *chiral* domains and the ellipticity of the envelope. The former was given by the least squares refinement as 0.504(2), 0.496(2) and the latter was insignificant. The absolute value of the Fe moment cannot be determined from the polarimetric data alone, as a close inspection of Eq. (4.2) will show. This can, however, be determined from the cross section Eq. (4.1) using the measured intensities. A least-squares fit of the data at 50 K was performed for the cycloid structure using the intensities of 11 satellites measured at this temperature. Assuming a circular cycloid, the only adjustable parameter of this fit is the value of the ordered Fe moment. The form factor of elemental Fe was used in the calculation of the cross section. The best fit was obtained with a value for the Fe moment of 1.10(3) μ_B. The improvement of the fit obtained by allowing some ellipticity is only marginal and it is therefore assumed that at 50 K the Fe cycloid is circular.

A similar analysis has been carried out on the first-order satellites of the magnetic modulation at 17 K. Here, both the Dy and Fe moments contribute to h and k odd reflections. This will affect *both* the intensities and the polarizations of the magnetic satellites. Equation (4.5) shows that in such case the scattering *amplitude* is a linear combination of the contribution from the two magnetic atoms, with coefficients depending on both the magnitude and direction of the vector coefficients **A** and **B** of the Fe and Dy modulations, and on the relative phase of the two modulations. There can be strong interference between the Dy and Fe which is crucial in determining the reflection intensities. The effect of this interference on the temperature dependence of the scattered intensity is addressed in a later section. A refinement of the magnetic structure at 17 K taking into account both the intensity and polarimetric data shows that the Dy atoms order in an elliptical cycloid rotating in the *opposite* sense to that of the Fe modulation. The major axis is parallel to the propagation vector and the ellipticity (ratio between the components parallel and perpendicular to the propagation vector) at 17 K is $\epsilon = 1.57$. The Fe modulation remains practically unchanged at all temperatures. Using fixed phases for the Fe atoms as given in Eq. (4.11), the best fit to the data was with the phase of the Dy atom at the origin equal to 42°.

A similar refinement of the 1.8 K data set was performed and the results of the best fit are shown in Table III. This shows that the phase relation between the two cycloids does not change significantly with temperature but the ellipticity of the Dy modulation does. At 1.8 K the ellipticity $\epsilon = 0.62$, i.e., the major axis of the helix envelope is now perpendicular to the propagation vector. Although there was not enough time to make polarimetric measurements at intermediate temperatures, it seems probable from these results that the ellipticity changes continuously with temperature. Indeed in a recent resonant x-ray magnetic scattering (RXMS) experiment performed on the same crystal the cycloidal nature of the rare-earth ordering was confirmed and it was found that at 12 K the envelope was closely circular.[11]

TABLE III. Parameters of the model of the magnetic structure of $DyFe_4Al_8$ and $HoFe_4Al_8$. The axis of the elliptical envelope of the rare-earth modulation are defined such that $\mu_\parallel \| [110]$ and $\mu_\perp \| [1\bar{1}0]$. The ellipticity is $\epsilon = \mu_\parallel / \mu_\perp$. The values of the moments are in μ_B.

	μ(Fe)	$\mu_\parallel$(M)	$\mu_\perp$(M)	ϵ	ϕ
$DyFe_4Al_8$					
50 K	1.06(4)	0	0		
17 K	=	1.54(3)	0.98(4)	1.57(5)	42°(6)
1.8 K	=	2.36(9)	3.77(8)	0.63(1)	=
$HoFe_4Al_8$					
70 K	0.96(2)	0	0		
20 K	0.98(3)	2.7(2)	3.6(3)	0.75(8)	150°(11)
2.4 K	1.06(3)	3.3(4)	6.4(4)	0.52(7)	149°(8)

V. TEMPERATURE DEPENDENCE OF THE STRUCTURE

We turn now to an analysis of the temperature dependence of the magnetic structure based on the thermal evolution of the magnetic satellites, interpreted within the framework of our model.

As discussed at the end of Sec. III A and shown in Figs. 5 and 6, the evolution with temperature of the intensity of the 110^+ satellite is remarkably different in the two compounds. In $HoFe_4Al_8$, the intensity of this reflection goes through a maximum at 70 K, decreases down to a minimum value at 23 K and increases in intensity again below that temperature, a behavior which is the reverse of that observed on $DyFe_4Al_8$. In contrast, the thermal behavior of the 121^+ satellite increases smoothly with decreasing temperature.

Recall that the 121^+ satellite is sensitive *only* to the rare-earth moment, and its intensity is simply proportional to the square of the $4f$ moment. The scale factor relating the intensities and the moments is known from an accurate measurement of the nuclear data set and, therefore, the evolution with temperature of the rare-earth moment is easily derived from the measured integrated intensity of this reflection as function of temperature. Although the thermal dependence of this reflection looks unexceptional at a first sight it is interesting to notice that the $I(T)$ curve has an exponential tail above 30 K that we could follow up to 60 K. This is not the expected critical behavior for a magnetic reflection and, probably, a small but finite moment exists on the rare earth below the ordering temperature of the Fe atoms. This can be explained by the nonvanishing local field created by the Fe atoms at the $2a$ sites. Such a small polarization of the Dy moment below T_N was seen through the polarization of the Dy $5d$ electrons in the RXMS experiment quoted previously.[11] Above 60 K the intensity of the 121^+ satellite is weak and we estimate an upper limit for the ordered $4f$ moment of 0.1 μ_B per rare-earth atom in this temperature region.

A first explanation of the peculiar shape of thermal dependence of the intensity of the 110^+ satellite as shown in Fig.

6 could be that a spin reorientation of the Fe moments occurs when the rare-earth orders. However, this explanation is unlikely on the basis of the high stability of the Fe modulation when an external magnetic field is applied (see Sec. VII). Indeed, our cycloidal model for the magnetic structure provides a simple explanation for the temperature behavior of the 110 satellites observed on the two compounds. This is shown by the following analysis. The intensity of the 110^+ satellite was extrapolated to low temperature assuming no ordered moment on the rare-earth atoms, which is shown as a dashed line on Figs. 5 and 6. The Fe moment is almost saturated at 70 K with a value $\sim 1\ \mu_B$. From this curve and from the measured intensity of the 121^+ satellite we directly calculated the value of the ordered Fe and rare-earth moment at each temperature. These values were used to calculate the intensity of the 110 satellites from our model without introducing any extra parameters, keeping the relative phase of the two cycloids fixed at the value given from the least-squares refinements of Table III. The result of this calculation is shown as full lines on Figs. 5 and 6. It is rewarding to notice that the temperature behavior is nicely reproduced in the two cases, in particular the pronounced minimum observed at 23 K in $HoFe_4Al_8$.

It is easy to explain the two different types of behavior observed for $DyFe_4Al_8$ and $HoFe_4Al_8$, if one realizes that the intensity of the 110^+ satellite is not given by the sum of the intensities from the two sublattices but that it is the scattering *amplitude* of each sublattice that adds coherently. This gives rise to an interference term between the two magnetic sublattices in the cross section [Eq. (4.1)]. The sign of this interference term is given by the relative phase of the two modulations. If this interference term is negative, which occurs if $90 < \phi < 180°$ a minimum occurs for a certain value of the growing rare-earth moment in the low temperature region. We show in Fig. 8 simulation of the expected dependence of the intensity of the 110^+ satellite as function of the ordered rare-earth moment. If the two modulations are $\phi = 90°$ out of phase, the simple quadratic behavior occurs. The $\phi = 43°$ curve models the situation of $DyFe_4Al_8$, where a sharp increase of intensity is observed when the rare-earth moment starts to grow. The experimental points for $HoFe_4Al_8$ follow closely the curve for $\phi = 150$. This gives us confidence in our model and shows that the phase angle ϕ does not vary much with temperature.

In the case of $DyFe_4Al_8$, we also observed a sharp decrease with temperature of the intensity of the 110^+ satellite below 10 K, at the onset of the higher-order satellites. As some of the moment contributes now to the higher order harmonics, a small decrease of the intensity of the first harmonic may be expected. This is not included in the model, which does not consider higher-order components.

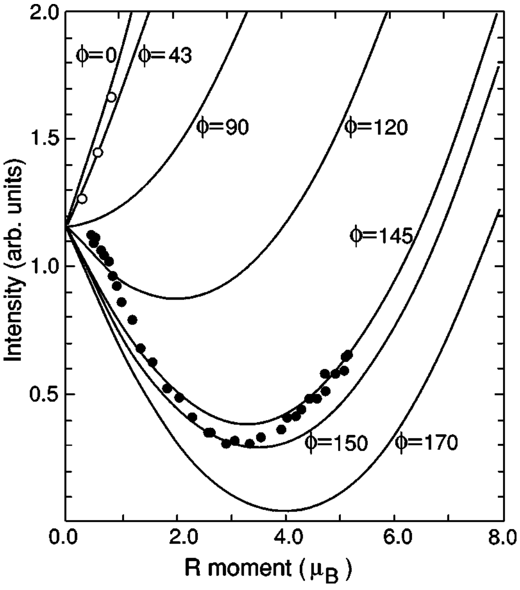

FIG. 8. Simulation of the intensity of the 110^+ satellite according to the model discussed in the text, as a function of the rare-earth moment. The open and filled circles are experimental data for $DyFe_4Al_8$ and $HoFe_4Al_8$, respectively. Solid lines are the results of the simulation for a fixed value of the Fe moment ($1\ \mu_B$) and for various phase offsets ϕ of the modulation of the rare-earth sublattice [the phases of the modulation of the Fe atoms are fixed according to Eq. (4.11)].

VI. MODELS OF THE STRUCTURE AT LOW *T*

Above 15 K the magnetic structure of $DyFe_4Al_8$ is relatively simple as the magnetic modulation can be described by a single harmonic. Figure 9 illustrates this structure as determined from the intensities and polarimetric data measured at 17 K. The special features of the neutron scattering which appear below 10 K are the satellites corresponding to higher harmonics of the propagation vector, and the strong diffuse scattering which gives evidence for ferromagnetic correlations between near neighbor Dy atoms. Polarimetric data gathered at 1.8 K on satellites corresponding to the third and fifth harmonics have been analyzed and give the ellipticities of the envelopes of the associated modulations. It was found that the third harmonic modulation had opposite ellipticity to those of the first and fifth. The numerical values of the ellipticities together with their respective amplitudes are given in Table IV. In analogy with what has been found in other rare earth alloys it is expected that the higher harmon-

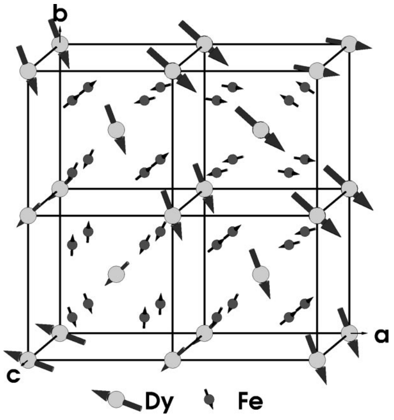

FIG. 9. Model of the magnetic structure of $DyFe_4Al_8$ at 17 K. At this temperature only one harmonic of the modulation is observed. The propagation direction is (110), the Fe moments are rotating clockwise and the Dy moments anticlockwise. There is another equivalent domain with the cycloid propagating along $[1\bar{1}0]$. The modulations of the sublattices of Fe atoms separated by $0,\frac{1}{2},0$ or $\frac{1}{2},0,0$ differ in phase by 180°.

TABLE IV. Higher harmonics of the magnetic structure of $DyFe_4Al_8$ at 1.8 K. The phases are relative to the first-order harmonic.

Harmonic	1		3		5	
component	[110]	$[1\bar{1}0]$	[110]	$[1\bar{1}0]$	[110]	$[1\bar{1}0]$
Ellipticity	0.63(1)		1.43(5)		0.52(5)	
Amplitudes	2.36	3.77	3.00	2.10	1.09	2.09
Phases	0	90	0	−90	180	−90

ics arise from some kind of bunching of the moment directions due to competition between the exchange and anisotropy within the rare-earth sublattice and the modulated molecular field due to Fe. It is unfortunately not possible to deduce the form of the bunching directly from the measurements, since the relative phases of the different modulations are not known. Figure 10 shows some of the patterns that are obtained by making different choices of these phases. Amongst the many patterns generated one, marked with an asterix in Fig. 10, displays some of the properties which might be expected from the physics of this system. Neighboring Dy atoms are coupled nearly ferromagnetically in pairs with successive pairs nearly parallel and perpendicular to the propagation vector, to maintain the periodicity this structure is faulted at every 15th Dy atom (those enclosed in circles) which has no ferromagnetically aligned neighbor. In the *periodic* part of the structure the Dy pairs are not exactly parallel, nor are they able to achieve their full amplitude. It may be conjectured that the diffuse scattering arises from random, possibly dynamic, fluctuations in the periodic structure which allow, on average, better ferromagnetic correlation between Dy pairs.

An alternative representation of the same model (marked with an asterisk in Fig. 10) and showing more clearly the lengths and directions of the moments is shown in Fig. 11.

VII. EFFECTS OF APPLIED MAGNETIC FIELD

The magnetic structure of $DyFe_4Al_8$ was studied under an applied magnetic field in two experiments conducted at the DR3 reactor of Risø National Laboratory. The sample was mounted with the $[1\bar{1}0]$ axis along the vertical field of a 5 T cryomagnet. Figure 12 shows the evolution with the field of the 0.5,0.5,0→2.5,2.5,0 scan. The results may be summarized as follows. With increasing fields there is an initial steep increase in the intensity of the magnetic first-order satellites of both 110 and 220 reflections, and then a decrease. From 0.75 T and above the satellites of the 220 reflection are no longer visible, and the satellites of the 110 reflection level off to an intensity comparable to that measured in zero field.

These results are interpreted as showing that at very low fields the modulation of the rare-earth moment is severely distorted, probably to a fanlike structure, with a ferromagnetic component aligned with the field. At around 0.75 T the modulation of the rare-earth moment is quenched. The $4f$ moments then align ferromagnetically parallel to the field, and their magnetic intensity appears at $\tau=0$; thus an increase in intensity of both 110 and 220 reflections is observed. Simultaneously, the pattern of diffuse scattering disappears. It is striking that the magnetic structure of the Fe sublattice remains unperturbed by the applied field up to the maximum value of 5 T. This is in agreement with the measured magnetization curves.

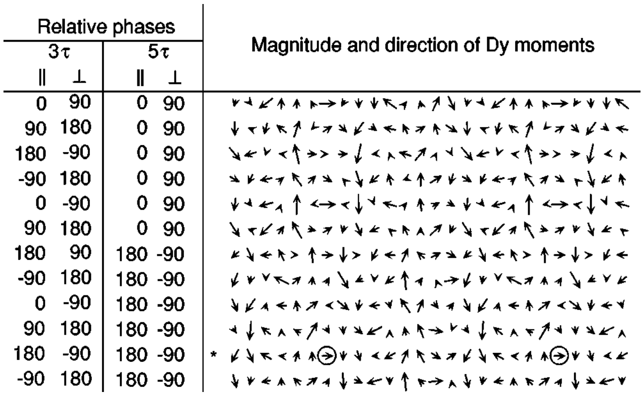

Relative phases				
3τ		5τ		
∥	⊥	∥	⊥	
0	90	0	90	
90	180	0	90	
180	-90	0	90	
-90	180	0	90	
0	-90	0	90	
90	180	0	90	
180	90	180	-90	
-90	180	180	-90	
0	-90	180	-90	
90	180	180	-90	
180	-90	180	-90	*
-90	180	180	-90	

FIG. 10. Magnitude and direction of the Dy spins, which correspond to different choices of the relative phases of the cycloids on the first, third and fifth harmonics in $DyFe_4Al_8$. Their positions are projected onto the [110] axis. The phases of the third and fifth harmonics for each arrangement are given relative to phases of 0 and 90° for the ∥ and ⊥ components of the first. The arrangement marked * is that described in the text; the Dy spins at positions at which the faults in this arrangement occur are encircled.

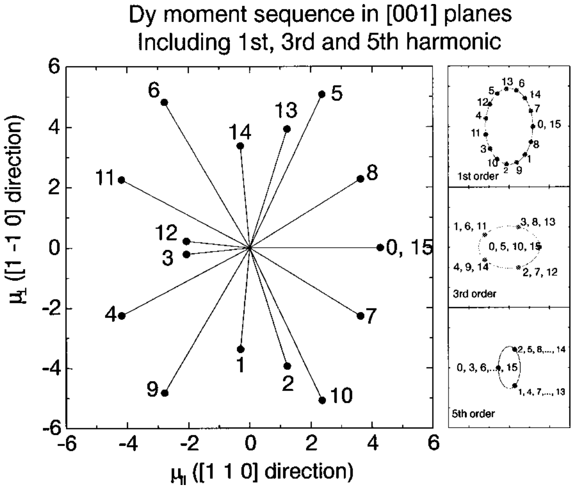

FIG. 11. Moment sequence for the Dy atoms only in the cycloid magnetic structure of $DyFe_4Al_8$ marked by * in Fig. 10. All Dy atoms along [110] directions have been projected to the same point. The numbered arrows show the length and direction of all moments in the individual planes perpendicular to the propagation direction. The rotation is in the [001] plane. The individual contributions to the total moment of the first, third, and fifth harmonics are shown as the ellipsoidal numbered points in the right hand figures.

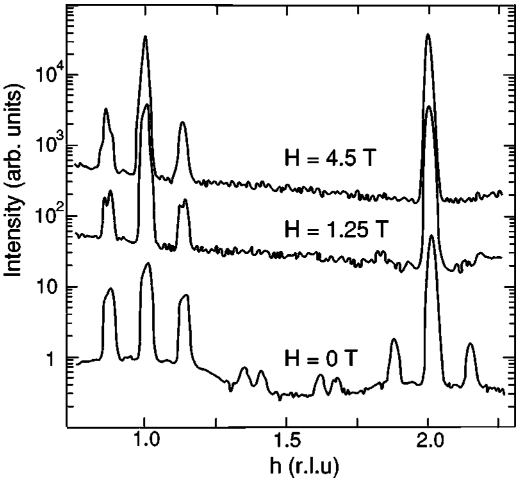

FIG. 12. Evolution with applied magnetic field of a longitudinal scan along the (110) reciprocal lattice direction of $DyFe_4Al_8$. The base lines of the scans at successsively higher fields are displaced by factors of 10^2. All the scans were measured at a temperature of 4.2 K, using the triple-axis spectrometer TAS1 at Risø with $\lambda = 4$ Å.

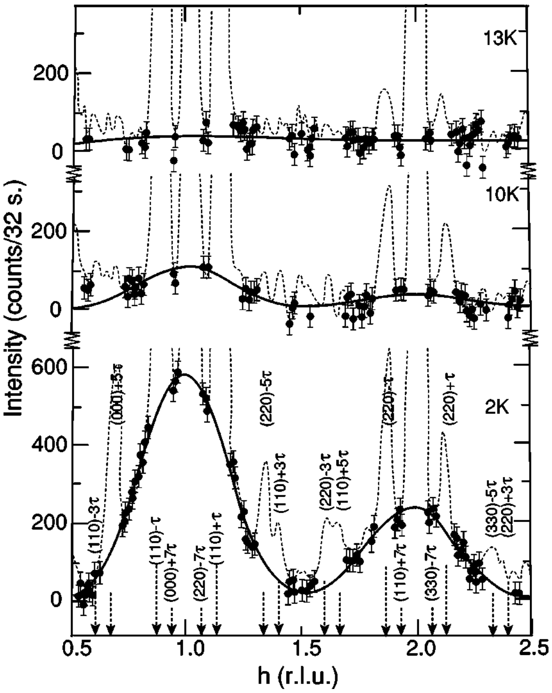

FIG. 13. Evolution with temperature of the diffuse scattering measured in longitudinal scans along (110) in $DyFe_4Al_8$. The dashed curves indicate the full profiles and the solid curves follow the diffuse background. Data measured on TAS3 at Risø and incident neutrons of $\lambda = 2.36$ Å.

VIII. DIFFUSE SCATTERING

Strong diffuse scattering beneath the Bragg peaks was observed well below the ordering temperature of the Dy sublattice in all experiments (Fig. 3). The diffuse scattering is centred around every reciprocal point of the *bct* lattice and extends over the whole Brillouin zone. The heights of these broad peaks of diffuse scattering were extracted from Gaussian fits. The variation of the intensity with temperature of the diffuse scattering is shown in Fig. 13. The diffuse scattering is attributed to short-range ferromagnetic correlations in the sample. After correction for geometric factors and the Dy^{3+} form factor, the intensities at the 110 and 220 positions are similar which indicates that the diffuse scattering comes from the rare-earth atoms only. It is closely linked to the long-range modulation of the rare-earth sublattice and disappears on application of the same small magnetic field that destroys this modulation while leaving that of the Fe sublattice unperturbed. The diffuse scattering integrated over the whole of the Brillouin zone represents a significant fraction of the Dy moment. It is estimated to be of the order of $3\mu_B$, which, taken with the antiferromagnetic component of $6\mu_B$, gives the full moment of the rare-earth ion Dy^{3+}. A simple calculation of the correlation length, based on the width of the peaks gives an estimate of 5 Å, which is about the distance between two neighboring Dy atoms in the structure. The width of the diffuse peaks perpendicular to the *ab* plane is small.[16] It was measured by performing transverse scans along the *c* axis through the 1.21 1.21 0 reciprocal lattice point, and along this direction was found to be resolution limited, indicating that the correlations occur only in the basal plane. We have also measured the quasielastic linewidth by scanning the energy at fixed momentum transfer at the reciprocal lattice positions 1.21,1.21,0; 1.5,1.5,0 and 1.77,1.77,0 between 1.7 and 5.8 K. These peaks had a Lorentzian line shape and all had widths larger than the resolution of the spectrometer determined from the incoherent scattering from a vanadium sample. (Further details are given in Ref. 16.)

IX. DISCUSSION

We summarize below the main results concerning our study of the magnetic structure of $DyFe_4Al_8$ and $HoFe_4Al_8$. The Fe sublattice orders on both compounds at ~175 K on a modulated structure which is a small modification of the G-type $+-+-$ AF structure propagating along (110). Superimposed on this simple antiferromagnetic order there is a long-wavelength modulation of the moments with $\boldsymbol{\tau} = \tau, \tau, 0$. The moments lie on the basal plane of the tetragonal unit cell and the moments rotate on this plane following a cycloid with a circular envelope. The value of the ordered Fe moment in both $DyFe_4Al_8$ and $HoFe_4Al_8$ is close to 1.0 μ_B. This value, although only 50% of that in bcc iron is consistent with measurements in other compounds with the $ThMn_{12}$ type of structure. The measured hyperfine field at the Fe nuclei is 11.0 T and the approximate relation of 12.7 T/μ_B is expected to hold for the $8f$ sites[17] for these compounds. The value obtained for the Fe moment is similar to the ordered Fe moment in UFe_4Al_8 and $UFe_{10}Si_2$.[17]

It is important for the discussion to notice that the rare-earth atoms are surrounded by eight Fe atoms located at the vertices of a tetragonal prism where the rare-earth atom is located at its center Fig. 1. For a G-type antiferromagnetic structure the local field exactly cancels out at the rare-earth site. This is no longer the case for a cycloid, but due to the long wavelength of the modulation the local field at the rare-earth site is small, although finite. Thus, one would expect a small moment to exist on the rare-earth below T_N, induced by the local field of the Fe sublattice. Although our neutron-experiments are not sensitive enough to show this small induced moment, the recent RXMS experiments on $DyFe_4Al_8$ support this reasoning. The polarization of the Dy $5d$ bands was followed as function of temperature and it was found that the $5d$ band polarizes simultaneously with the ordering of the Fe atoms.

Around ~50 K the rare-earth moment orders, and the ordered moment rises sharply at low temperature. Interestingly, a charge modulation of wavevector $2\boldsymbol{\tau}$ was seen to develop on $DyFe_4Al_8$ at this temperature.[11] This shows that there is a strong magnetoelastic coupling between the rare-earth moments and the lattice, which also manifests itself as a noticeable reduction of the extinction of the rather perfect single crystal below the ordering temperature of the rare earth. The wave vector is the same for both the Fe and rare-earth modulations, which also points to some coupling between the two sublattices. This coupling is, however, relatively weak as a small applied magnetic field induces major changes in the magnetic ordering of the rare-earth sublattice, leaving that of the Fe atoms unchanged. Our results, in particular the polarimetric measurements, exclude any component of the moments out of the basal ab plane, in disagreement with previous models proposed for $DyFe_4Al_8$.[4] The neutron results are in agreement with the low value of the susceptibility measured along the tetragonal c axis.

At low temperature, the cycloid is unstable as shown by the appearance of extra satellites corresponding to higher-order harmonics of the magnetic modulation. This is understandable from entropic arguments, and such harmonics would correspond to a bunching of the moments into particular directions due to competition between exchange and anisotropy terms in the free energy.

Interestingly, a non-negligible fraction of the moment of the rare-earth remains disordered at low temperature, particularly in the case of $DyFe_4Al_8$. This disordered moment gives rise to a broad pattern of diffuse scattering beneath the Bragg peaks below the temperature at which the bunching of the cycloid occurs. A most likely explanation for the diffuse scattering is that it is due to ferromagnetic correlation between Dy pairs originating from random fluctuations in the periodic structure. An energy-analysis of this diffuse scattering has shown that it is quasielastic. From the Lorentzian line shape and finite width of this quasielastic scattering one may conclude that the short-range order correlations giving rise to the diffuse scattering are not static but fluctuate in time. This point deserves a more thorough investigation in the future.

X. CONCLUSIONS

We report the results of neutron-scattering experiments performed on well characterized single crystals which have provided a detailed picture of the magnetic structure of $DyFe_4Al_8$ and $HoFe_4Al_8$. These two compounds are representative of the family of $M\mathrm{Fe}_4\mathrm{Al}_8$ compounds with the $ThMn_{12}$-type of structure whose interesting magnetic properties have, up to now, remained largely unexplained in spite of much experimental effort and numerous contradictory interpretations. The neutron-scattering experiments reported in this paper show that both the Fe and rare-earth sublattices have long-range magnetic order and most of the unusual properties which have been attributed to a spin-glass state are explained by the cycloidal ordering of the magnetic atoms. The unusual thermomagnetic effects and hysteretic behavior, which have puzzled so many authors, are simply explained by the high degree of sensitivity of the modulated magnetic structure of the rare-earth sublattice to small applied magnetic fields. In some of the earlier investigations (Refs. 5 and 9) the Fe sublattice was not completely ordered to the extent of between 5 and 10%. It remains to be seen whether such concentration differences alter substantially the magnetic behavior.

To conclude, this study shows that atomic probes of magnetism, such as neutron scattering, performed on well characterized single crystals are clearly needed to understand such a complex magnetic behavior as that exhibited by this family of compounds.

ACKNOWLEDGMENTS

J.A.P. and M.R.S. acknowledge the support provided under the Training and Mobility of Researchers – Large Installation Program of the European Union to perform the neutron scattering experiments at Risø. J.A.P. acknowledges the Institute for Transuranium Elements, Karlsruhe, for providing some travel funds. We are indebted to Professor Margarida Godinho of University of Lisbon for use of the SQUID magnetometer and to G. McIntyre for his help on the experiments on D10. This work is part of a project financed by JNICT/FCT under Contract No. PBIC/FIS/2213/95.

---

[1] K.H. Buschow and A.M. van der Kraan, J. Phys. F: Met. Phys. **8**, 921 (1978).

[2] I. Felner and I. Nowik, J. Phys. Chem. Solids **39**, 951 (1978).

[3] P.C.M. Gubbens, A.M. van der Kraan, and K.H.J. Buschow, J. Magn. Magn. Mater. **27**, 61 (1982).

[4] W. Schäfer and G. Will, J. Less-Common Met. **94**, 205 (1983).

[5] J. Gal, I. Yaar, E. Arbaboff, H. Etedgi, F.J. Litterst, K. Aggarwal, J.A. Pereda, G.M. Kalvius, G. Will, and W. Schäfer, Phys. Rev. B **40**, 745 (1989).

[6] W. Schäfer, G. Will, G.M. Kalvius, and J. Gal, Physica B **156-157**, 751 (1989).

[7] E. Talik, J. Szade, and J. Heinmann, Physica B **190**, 361 (1993).

[8] E. Talik, J. Heinmann, J. Szade, and T. Mydlarz, Physica B **205**, 127 (1995).

[9] J. Gal, I. Yaar, D. Regev, S. Fredo, G. Shani, E. Arbaboff, W. Potzel, K. Aggarwal, J.A. Pereda, G.M. Kalvius, F.J. Litterst, W. Schäfer, and G. Will, Phys. Rev. B **42**, 8507 (1990).

[10] J.A. Paixão, B. Lebech, A.P. Gonçalves, P.J. Brown, G.H. Lander, P. Burlet, A. Delapalme, and J.C. Spirlet, Phys. Rev. B **55**, 14 370 (1997).

[11] S. Langridge, J.A. Paixão, N. Bernhoeft, C. Vettier, G.H. Lander, Doon Gibbs, S.A. Sørensen, A. Stunault, D. Wermeille, and E. Talik, Phys. Rev. Lett. **82**, 2187 (1999).

[12] P. Becker and P. Coppens, Acta Crystallogr., Sect. A: Cryst.

Phys., Diffr., Theor. Gen. Crystallogr. **30**, 129 (1974).

[13] P.J. Brown, J.B. Forsyth, and F. Tasset, Proc. R. Soc. London, Ser. A **442**, 147 (1993).

[14] M. Blume, Phys. Rev. **130**, 1670 (1960).

[15] V. Nunez, P.J. Brown, J.B. Forsyth, and F. Tasset, Physica B **174**, 60 (1991).

[16] S. Aagaard Sørensen, Risø Report No. Risø-R-1125 (EN), 1999 (unpublished).

[17] J.A. Paixão, J.C. Waerenborgh, M.S. Rogalski, A.P. Gonçalves, M. Almeida, A. Gukasov, M. Bonnet, J.C. Spirlet, and J.B. Sousa, J. Phys.: Condens. Matter **10**, 4071 (1998).